Japan Journal of
Astronomy and Astrophysics

Academixs
Open Access Publishers

Research Article

# Experimental Investigation of Aluminum 1100 Cladding on SCM440 Steel Using GTAW: Effects of Welding Current and Feed Rate on Cracking, Microstructure, and Mechanical Properties

**Paisan Thongsong[1*] and Kittipong Kimapong[2]**

[1,2]*Department of Industrial Engineering, Rajamangala University of Technology Thanyaburi (RMUTT), Thailand*

***Corresponding Author:**
Paisan Thongsong. Department of Industrial Engineering, Rajamangala University of Technology Thanyaburi (RMUTT), Thailand.

**Received Date:** 26.01.2026 **Accepted Date:** 04.02.2026 **Published Date:** 09.02.2026

**Abstract**

*This study provides a systematic investigation into the combined effects of welding current (75–175 A) and wire feed rate (300–600 mm/min) on cracking behavior, solidification characteristics, and interfacial reactions during Gas Tungsten Arc Welding cladding of Aluminum 1100 onto SCM440 steel—a dissimilar material combination for which comprehensive microstructural analysis remains limited. The results reveal a clear transition from severe solidification cracking to crack-free clads as heat input increases, establishing 150–175 A as the threshold for molten pool stability. A coupled evaluation of dendrite arm spacing, hardness, and interfacial diffusion further highlights the sensitivity of Fe-rich IMC formation to feed-rate-controlled heat input. Dendrite arm spacing increases with current but decreases with feed rate, while EDS analysis confirms the formation of Fe-rich intermetallic phases consistent with diffusion-driven Al–Fe reactions. The integrated mapping of cracking, DAS, IMC chemistry, and bead geometry identifies 150 A with 500 mm/min as an optimal condition for producing defect-free and metallurgically stable aluminum–steel clads. These findings offer new insights into heat-input–controlled phase evolution and provide a practical framework for optimizing GTAW-based aluminum cladding on alloy steels.*

**Keywords:** GTAW Cladding, Aluminum 1100, SCM440, Intermetallic Compounds, Dendrite Arm Spacing, Cracking Behavior

## Introduction

Dissimilar joining between aluminum and steel has grown increasingly important due to the demand for lightweight structures and corrosion-resistant surfaces. However, joining these materials remains challenging because of significant differences in melting temperature, thermal expansion, and the formation of brittle Fe–Al intermetallic compounds (IMCs). Recent reviews confirm that IMCs such as Fe2Al5 and FeAl3 form readily and are detrimental to joint toughness [1-7]. Studies also demonstrate that heat input governs IMC morphology and thickness, influencing mechanical performance [8-12].

Furthermore, the interfacial Fe–Al layer formed during welding is known to be hard and brittle, contributing to interfacial cracking and poor ductility [8,9]. Managing heat input, arc behavior, and thermal gradients is therefore crucial for producing crack-free aluminum–steel joints [13, 14].

Hasanniah et al. showed that pulsed GTAW of aluminum-clad steel is highly sensitive to welding current and wire feed rate, which affect molten pool stability and bead characteristics [15]. Additional work has demonstrated that solidification parameters such as dendrite arm spacing (DAS) strongly influence hardness and microstructural refinement [12,16-18].

Although various welding technologies—including laser welding, friction-based joining, and hybrid welding-brazing—have been studied for aluminum–steel joining investigations focused specifically on GTAW cladding of commercially pure Aluminum 1100 on SCM440 remain limited [4-6]. Several hybrid welding studies also highlight the advantages of combining arc and friction-based processes to control IMC formation and improve joint integrity [18]. Additionally, prior work by Thongsong et al. demonstrated that GTAW cladding on SCM440 can achieve refined microstructures and stable clad geometry under controlled heat input, supporting the relevance of the present investigation [19]. This study aims to bridge this gap by experimentally analyzing cracking behavior, DAS

evolution, hardness distribution, and interfacial IMC formation.

## Experimental Methodology

SCM440 low-alloy steel plates (150 × 100 × 20 mm) with chemical composition shown in Table 1, were used as substrates, and Aluminum 1100 wire (1.2 mm diameter) served as the filler metal. GTAW was performed in DCEN mode using a 2.4 mm thoriated tungsten electrode with an 80° torch angle, 2 mm arc length, and 15 L/min argon shielding gas (Figure 1). Welding parameters varied in this study included current levels of 75, 100, 125, 150, and 175 A, along with wire feed rates of 300, 400, 500, and 600 mm/min; the cladding was performed at room temperature.

**Table 1: Chemical composition of materials**

| Element | SCM440 | ER1100 |
|---|---|---|
| Fe | Bal. | 0.20 |
| C | 0.40 | - |
| Si | 0.10 | 0.25 |
| Cr | 0.91 | - |
| Al | - | Bal. |

Macrostructural and microstructural examinations were carried out using optical microscopy. Surface crack count was evaluated at 50× magnification, hardness was measured using the Vickers method (50 g load, 10 s dwell), dendrite arm spacing (DAS) was quantified using ImageJ, and the chemical composition of the clad metal (CM) was analyzed at the middle position through EDS.

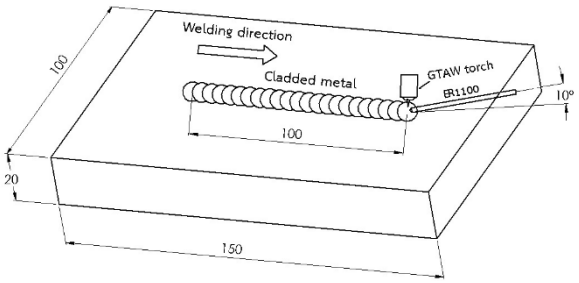


**Figure 1:** Schematic of cladding method

## Results and Discussion

### Crack Formation Behavior

Table 2 summarizes the cracking severity observed in the clad metal under various welding conditions. At low welding currents (75–100 A), severe cracking and incomplete wetting were frequently observed, as illustrated in Figure 2(a). This behavior is attributed to thermal mismatch between aluminum and steel, which generates high tensile stresses during rapid solidification, as well as insufficient heat input that leads to unstable molten pool behavior [,18,9,13,19]. The limited fusion and fast cooling at these low currents promote the formation of brittle interfacial regions where cracks readily initiate.

In contrast, increasing the welding current to 150–175 A produced fully crack-free clads, as shown in Figure 2(b). The enhanced heat input stabilizes the molten pool, improves wetting behavior, and reduces thermal gradients, thereby suppressing crack formation. Similar improvements in crack resistance with higher heat input were also reported by Hasanniah et al. for aluminum–steel GTAW cladding [15].

Feed rate also played an important role: higher feed rates (>500 mm/min) promoted cracking at low welding currents because of lower effective heat input per unit length and accelerated cooling, both of which limit fusion and amplify thermal stress concentrations.

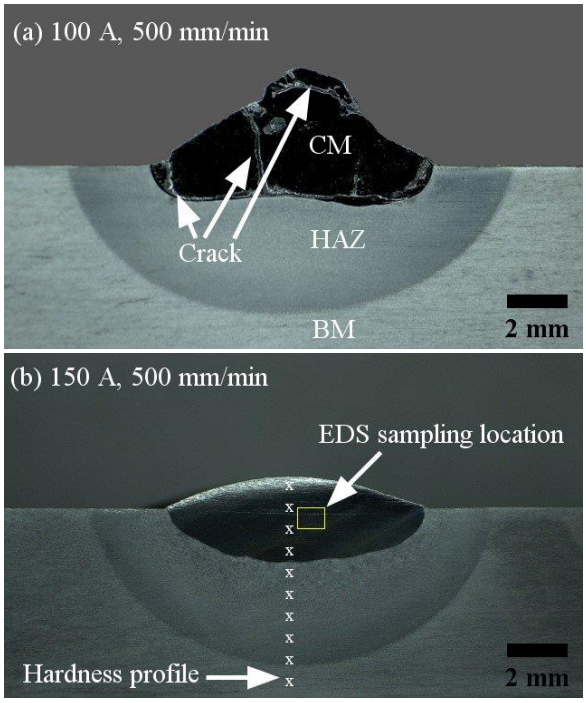


**Figure 2:** Macrostructure of samples (a) 100 A 500 mm/min, (b) 150 A 500 mm/min

**Table 2: Surface crack count for each parameter**

| Current | Feed rate (mm/min) | | | |
|---|---|---|---|---|
| (A) | 300 | 400 | 500 | 600 |
| 75 | 7 | 8 | 15 | 15 |
| 100 | 0 | 3 | 10 | 14 |
| 125 | 0 | 0 | 5 | 3 |
| 150 | 0 | 0 | 0 | 0 |
| 175 | 0 | 0 | 0 | 0 |

**Dendrite Arm Spacing (DAS) Analysis**

The variation in dendrite arm spacing under different welding parameters is further illustrated in Figure 3(a–d). The microstructures reveal that at lower welding currents (e.g., 75–100 A), the rapid solidification results in finer dendritic structures, while higher currents promote coarser dendrite arm spacing due to reduced cooling rates, consistent with solidification models reported in the literature [12,16,17].

Figure 4 shows the relationship between welding current and DAS, demonstrating a clear increasing trend as the current rises from 75 A to 175 A. The minimum DAS (~2.3 μm) occurs under conditions of low heat input and high feed rate, aligning with the fine dendritic patterns visible in Figure 3 (a–b). Conversely, the coarser dendritic structure observed in Figure 3(c–d) corresponds to higher heat input levels, where slower cooling promotes larger dendrite arm spacing, in agreement with prior observations in aluminum solidification studies [16], [18]. Higher wire feed rates produced smaller DAS due to reduced heat per unit length. The smallest DAS observed, aligned with trends reported in high cooling rate Al/steel welds (~2.3 μm) correlates with microstructural refinement trends reported in rapid solidification aluminum welds [4,5,12,18].

**Hardness Distribution**

The hardness profiles measured from the base metal (BM) through the heat-affected zone (HAZ) and into the weld metal are shown in Figure 5. The hardness increase observed in the HAZ—often higher than that of the weld metal—is attributed to the transformation of the SCM440 steel microstructure from ferrite + pearlite into martensite due to rapid cooling during welding. This behavior is consistent with metallurgical phase transformation principles reported in prior Al–steel welding studies [8,9,18]. In contrast, hardness within the weld metal is primarily affected by dendritic refinement and controlled IMC formation, with moderate weld-metal hardness was observed under welding currents of 125–150 A, in agreement with previous GTAW cladding studies [15,18].

Furthermore, Figure 5 highlights the effect of wire feed rate on weld metal hardness at a constant welding current of 150 A. As the feed rate increased from 300 to 600 mm/min, the hardness of the weld metal showed a clear decreasing trend. The maximum weld metal hardness of approximately 384 HV was recorded at a feed rate of 300 mm/min, whereas the minimum hardness of about 302 HV occurred at 600 mm/min. This behavior reflects the influence of heat input per unit length—higher feed rates

reduce effective heat input, leading to insufficient fusion and coarser microstructure, which ultimately lowers weld metal hardness, matches trends reported by observations in prior aluminum solidification and cladding studies [16-18].

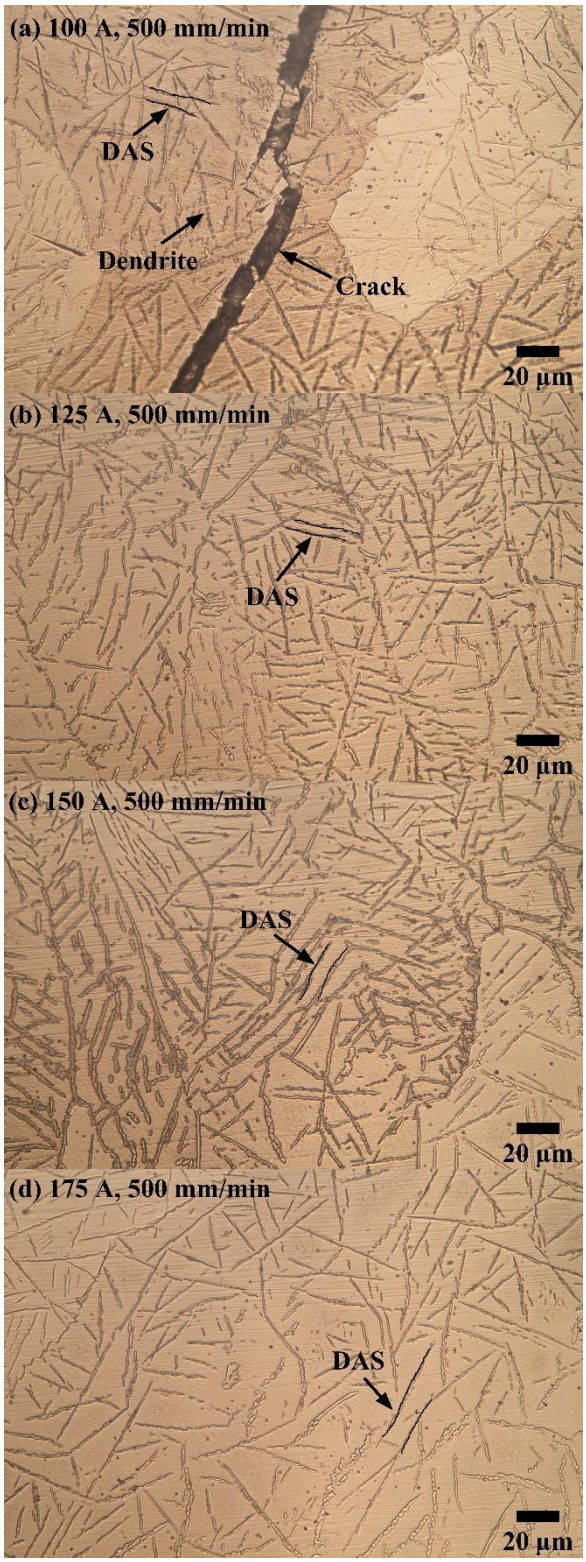


**Figure 3:** Samples of the microstructure of the clad metal

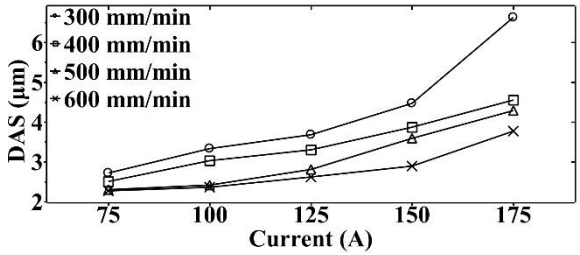


**Figure 4:** Relationship between DAS and welding current

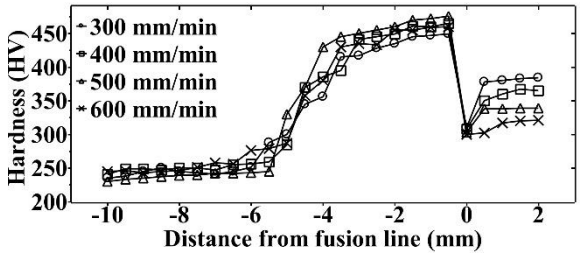


**Figure 5:** Hardness profiles of the clad metal at a welding current of 150 A

## Weld Geometry (W/H and W/P)

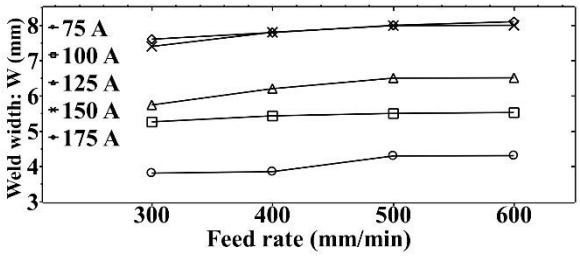


**(a) weld width (W)**

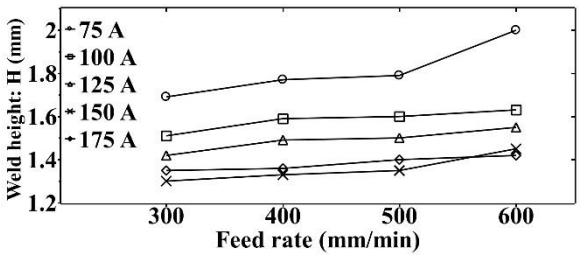


**(b) weld height (H)**

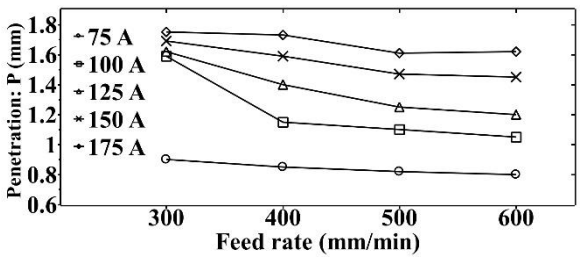


**(c) penetration (P)**

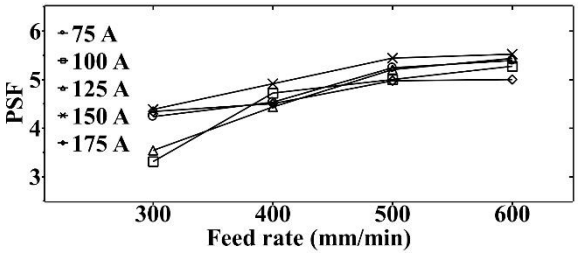


(d) PSF (W/P)

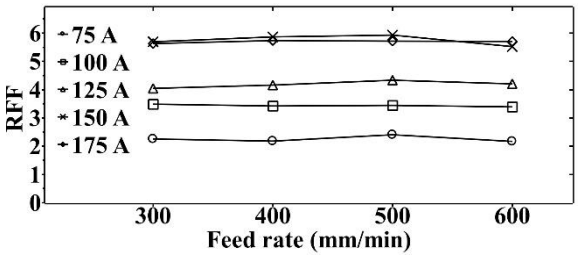


(e) RFF (W/H)

**Figure 6:** Relationship between feed rate and weld geometry: (a) weld width (W), (b) weld height (H), (c) penetration (P), (d) PSF (W/P), and (e) RFF (W/H)

The geometric characteristics of the clad metal under different welding conditions are illustrated in Figure 6(a–e). Figure 6(a) presents the weld width (W), which increases with higher welding currents due to enhanced molten pool spreading and improved wettability, consistent with observations in previous GTAW studies [15,18]. Figure 6(b) shows the weld height (H), where reinforcement tends to increase at lower feed rates as more filler metal accumulates per unit length.

The weld penetration depth (P), shown in Figure 6(c), increases with welding current because of higher arc energy density, which promotes deeper heat transfer into the substrate. This trend aligns with reported thermal-fluid behavior in aluminum–steel GTAW processes [3,9].

Figure 6(d) illustrates the penetration shape factor (PSF) defined as the ratio W/P [20]. Higher PSF values indicate wider but shallower deposits, typically occurring under high feed rates or lower currents, where heat input per unit length is reduced. This shape factor is strongly influenced by molten pool stability and heat distribution across the clad width.

Figure 6(e) presents the reinforcement form factor (RFF) defined as the ratio W/H, where H is the reinforcement height [20]. Higher RFF values correspond to smoother and more uniform clad profiles, whereas lower values indicate excessive reinforcement or insufficient pool flattening. These geometric trends demonstrate how welding current and feed rate collectively influence bead morphology, which is critical for achieving high-quality aluminum cladding. Wider beads and deeper penetration were observed at higher currents, reflecting improved arc energy and wetting. Hasanniah et al. reported similar effects in GTAW aluminum cladding. High feed rates slightly reduced penetration due to lower heat input per unit length [15,18].

## IMC Formation (EDS)

**Table 3: Elemental composition of clad metal (at%)**

| Current (A) | Feed (mm/min) | Fe (at%) | Al (at%) | Fe/Al Ratio | Predicted IMC Phase |
|---|---|---|---|---|---|
| 75 | 300 | 73.75 | 25.13 | 2.93 | Fe3Al |
| | 400 | 72.02 | 26.88 | 2.68 | Fe3Al |
| | 500 | 68.49 | 30.43 | 2.25 | Fe3Al / FeAl |
| | 600 | 68.07 | 30.82 | 2.21 | Fe3Al / FeAl |
| 100 | 300 | 74.12 | 24.79 | 2.99 | Fe3Al |
| | 400 | 72.59 | 26.34 | 2.75 | Fe3Al |
| | 500 | 68.64 | 30.21 | 2.27 | Fe3Al / FeAl |
| | 600 | 68.37 | 30.56 | 2.24 | Fe3Al / FeAl |
| 125 | 300 | 74.49 | 24.41 | 3.05 | Fe3Al |
| | 400 | 72.82 | 26.06 | 2.79 | Fe3Al |

| | | | | | |
|---|---|---|---|---|---|
| | 500 | 68.88 | 30.01 | 2.29 | Fe3Al / FeAl |
| | 600 | 68.55 | 30.38 | 2.26 | Fe3Al / FeAl |
| 150 | 300 | 74.54 | 24.06 | 3.10 | Fe3Al |
| | 400 | 73.01 | 25.71 | 2.84 | Fe3Al |
| | 500 | 70.29 | 28.69 | 2.45 | Fe3Al / FeAl |
| | 600 | 68.47 | 30.11 | 2.27 | Fe3Al / FeAl |
| 175 | 300 | 75.03 | 23.85 | 3.15 | Fe3Al |
| | 400 | 73.42 | 25.46 | 2.88 | Fe3Al |
| | 500 | 69.57 | 29.33 | 2.37 | Fe3Al / FeAl |
| | 600 | 69.00 | 29.87 | 2.31 | Fe3Al / FeAl |

The EDS results in Table 3 show that the Fe content at the Al–Fe interface ranges from 68–75 at%, corresponding to Fe/Al ratios between 2.2 and 3.15. These values indicate that the intermetallic layer is dominated by Fe-rich phases such as Fe3Al and FeAl, which are typically observed in aluminum–steel welding [2,8,9]. Higher welding currents (150–175 A) produced the largest Fe/Al ratios, suggesting enhanced Fe diffusion into the molten aluminum due to increased heat input.

Fe-rich IMCs are significantly less brittle than Al-rich compounds (e.g., FeAl3), and their formation has been associated with reduced interfacial cracking in previous studies [8,9,18]. This agrees with the present results, where crack-free clads were obtained under higher heat input conditions that favor Fe-rich IMC formation.

Increasing feed rate slightly decreased Fe content and Fe/Al ratio, indicating reduced diffusion and potentially thinner IMC layers due to lower heat input per unit length. These trends are consistent with the hardness profiles, where lower feed rates produced higher interfacial hardness due to thicker Fe-rich IMC layers, while higher feed rates resulted in smoother hardness gradients.

Overall, the IMC formation behavior confirms that controlled heat input promotes the development of Fe-rich, mechanically favorable IMCs, which play a key role in achieving stable and crack-resistant aluminum–steel cladding [3,4,18].

## Conclusion

The optimal condition for GTAW cladding of Aluminum 1100 on SCM440 steel was identified as a welding current of 150 A combined with a wire feed rate of 500 mm/min. This parameter set produced crack-free clads together with a weld-metal hardness level that remains within an acceptable range for structural performance. In addition, the bead geometry under this condition exhibited high PSF and RFF values, indicating well-distributed reinforcement and stable molten pool behavior. The IMC formed under this condition consisted primarily of Fe-rich phases, contributing to balanced mechanical and metallurgical stability. Overall, the results confirm that 150 A with a feed rate of 500 mm/min offers the best combination of process stability, acceptable hardness, and high-quality weld geometry for Aluminum 1100 cladding on SCM440 steel.

## References


1. Yang, Y., Luo, Z., Zhang, Y., & Su, J. (2024). Dissimilar welding of aluminium to steel: A review. Journal of Manufacturing Processes, 110, 376-397.
2. Atabaki, M. M., Nikodinovski, M., Chenier, P., Ma, J., Harooni, M., & Kovacevic, R. (2014). Welding of aluminum alloys to steels: an overview. Journal for Manufacturing Science and Production, 14(2), 59-78.
3. Gullino, A., Matteis, P., & D'Aiuto, F. (2019). Review of aluminum-to-steel welding technologies for car-body applications. Metals, 9(3), 315.
4. Wallerstein, D., Salminen, A., Lusquinos, F., Comesana, R., García, J. D. V., Rodríguez, A. R., ... & Pou, J. (2021). Recent developments in laser welding of aluminum alloys to steel. Metals, 11(4), 622.
5. Li, Q., Yang, S., Hu, B., & Xue, S. (2025). Laser welding of aluminum/steel dissimilar metals and control of intermetallic compounds: a review. The International Journal of Advanced Manufacturing Technology, 1-26.
6. Pan, B., Sun, H., Shang, S. L., Banu, M., Wang, P. C., Carlson, B. E., ... & Li, J. (2022). Understanding formation mechanisms of intermetallic compounds in dissimilar Al/steel joint processed by resistance spot welding. Journal of Manufacturing Processes, 83, 212-222.
7. Yu, X., Fan, D., Huang, J., Li, C., & Kang, Y. (2019). Arc-assisted laser welding brazing of aluminum to steel. Metals, 9(4), 397.
8. M. Potesser, T. Schöberl, H. Antrekowitsch, and J. Bruckner, "The Characterization of the Intermetallic Fe-Al Layer of Steel-Aluminum Weldings," TMS Annual Meeting, vol. 2006, pp. 1-8.
9. Zhang, M., Wang, Y. D., Xue, P., Zhang, H., Ni, D. R., Wang, K. S., & Ma, Z. Y. (2022). High-quality dissimilar friction stir welding of Al to steel with no contacting between tool and steel plate. Materials Characterization, 191, 112128.
10. Kajihara, M. (2006). Quantitative evaluation of interdiffusion in Fe2Al5 during reactive diffusion in the binary Fe–Al system. Materials transactions, 47(6), 1480-1484.
11. Shang, S. L., Sun, H., Pan, B., Wang, Y., Krajewski, A. M., Banu, M., ... & Liu, Z. K. (2021). Forming mechanism of equilibrium and non-equilibrium metallurgical phases in dissimilar aluminum/steel (Al–Fe) joints. Scientific reports, 11(1), 24251.
12. NGotawala, N., & Shrivastava, A. (2021). Investigation of interface microstructure and mechanical properties of rotatory friction welded dissimilar aluminum-steel joints. Materials Science and Engineering: A, 825, 141900.
13. HSFL Carvalho, G., Galvão, I., Mendes, R., M. Leal, R., & Loureiro, A. (2020). Aluminum-to-steel cladding by explosive welding. Metals, 10(8), 1062.
14. Bolhasani Hesari, M., Beygi, R., Teixeira, T. O., Marques,

E. A., Carbas, R. J., & da Silva, L. F. (2025). Enhancing High-Temperature Durability of Aluminum/Steel Joints: The Role of Ni and Cr in Substitutional Diffusion Within Intermetallic Compounds. Metals, 15(4), 465.
15. Hasanniah, A., & Movahedi, M. (2018). Welding of Al-Mg aluminum alloy to aluminum clad steel sheet using pulsed gas tungsten arc process. Journal of Manufacturing Processes, 31, 494-501.
16. Davis, J. R. (1993). Aluminum and aluminum alloys. ASM Specialty Handbook/ASM International.
17. Zhang, G., Chen, M., Shi, Y., Huang, J., & Yang, F. (2017). Analysis and modeling of the growth of intermetallic compounds in aluminum–steel joints. RSC advances, 7(60), 37797-37805.
18. Liu, J., Wu, B., Wang, Z., Li, C., Chen, G., & Miao, Y. (2023). Microstructure and mechanical properties of aluminum-steel dissimilar metal welded using arc and friction stir hybrid welding. Materials & Design, 225, 111520.
19. Thongsong, P., Toonangkul, P., Triwanapong, S., & Kimapong, K. (2024). Single-pass GTAW cladding of aluminum clad metal on SCM440 low-alloy steel surface. Journal of Mechanical Science and Technology, 38(7), 3577-3583.
20. Mondal, A., Kumar Saha, M., Hazra, R., & Das, S. (2016). Influence of heat input on weld bead geometry using duplex stainless steel wire electrode on low alloy steel specimens. Cogent Engineering, 3(1), 1143598.

**Citation:** Thongsong, P., Kimapong, K., (2026). Experimental Investigation of Aluminum 1100 Cladding on SCM440 Steel Using GTAW: Effects of Welding Current and Feed Rate on Cracking, Microstructure, and Mechanical Properties. *Jpn. J. Astron. Astrophys. 2*(1), 1-8.